PCCP

PAPER

View Article Online
View Journal | View Issue

Cite this: *Phys. Chem. Chem. Phys.*, 2022, **24**, 15991

Delamination of MoS_2/SiO_2 interfaces under nanoindentation†

Jin Ke,‡ Penghua Ying,‡ Yao Du, Bo Zou, Huarui Sun and Jin Zhang *

Received 7th January 2022,
Accepted 6th June 2022

DOI: 10.1039/d2cp00074a

rsc.li/pccp

Molybdenum disulphide (MoS_2) mounted on silicon dioxide (SiO_2) constitutes the fundamental functional components of many nanodevices, but its mechanical properties, which are crucial for the device design and fabrication, remain almost unexplored. Here, the mechanical properties of the multilayer MoS_2/SiO_2 system are investigated *via* nanoindentation experiments and molecular dynamics simulations. In terms of the mechanical properties, a comparative study of MoS_2/SiO_2 and graphene/SiO_2 systems is presented. The MoS_2/SiO_2 and graphene/SiO_2 systems are found to possess comparable Young's modulus and hardness values, but their mechanical responses and failure modes under indentation are totally different. Interface delamination failure accompanied by ring-like through-thickness cracking is observed in the MoS_2/SiO_2 system with a relatively thin MoS_2 layer, while no interface separation is found in indentation experiments for the graphene/SiO_2 system using the same layer thickness. The different failure modes observed between the MoS_2/SiO_2 and graphene/SiO_2 systems can be attributed to the comparable interface adhesion energy but very different bending stiffness values of the MoS_2 and graphene components. Specifically, compared with graphene, the larger bending stiffness of MoS_2 means that a larger bending force is experienced in the indentation process, overcoming the adhesion of the MoS_2/SiO_2 interface, which makes interface delamination much easier in the MoS_2/SiO_2 system.

Introduction

Since mechanically exfoliated graphene was successfully fabricated in 2004,[1] two-dimensional (2D) materials have attracted increasing attention because of their unique properties that are superior to their counterpart bulk forms.[2] As an important member of the 2D materials family, transition metal dichalcogenides (TDMs) are regarded as alternatives to graphene because their band gap properties are different from those of graphene.[3–5] Among over 40 compounds found in the family of TMDs, molybdenum disulphide (MoS_2) has attracted a great deal of attention due to its promising potential in semiconducting applications.[6–8] Similar to graphene, neighbouring layers in MoS_2 are connected with each other by only weak van der Waals (vdW) forces, while the in-plane stability of each layer is sustained by strong chemical bonds. Monolayer and multilayer MoS_2 nanosheets are reported to have numerous remarkable thermal, mechanical, electrical and optical properties that promise revolutionary advances in the fabrication of transistors, sensors and flexible electronic devices.[6–10]

The fabrication of robust MoS_2-based nanodevices and the reliable operational performance of these nanodevices both rely crucially on the mechanical properties of MoS_2. The atomic force microscopy (AFM)-based nanoindentation of suspended MoS_2 nanosheets is a widely used technique to measure the intrinsic mechanical properties (*e.g.*, Young's modulus and fracture strength) of MoS_2.[11,12] The AFM-based nanoindentation method has also been extended to investigate the effects of film thickness,[13] phase transitions,[14] atomic vacancies,[15] and electromechanical coupling[16] on the mechanical properties of MoS_2. Other experimental techniques, such as bulge testing,[17] the buckling metrology method,[18] Brillouin light scattering,[19] bimodal AFM mapping,[20] and *in situ* tensile testing,[21] have also been developed to study the elastic deformation, fracture and bending of MoS_2. In addition to experimental methods, some atomic simulation methods including molecular dynamics (MD) simulations and first-principles calculations have been used to simulate the nanoindentation,[22,23] stretching,[24,25] and bending[26] processes of freestanding MoS_2. Results obtained from these simulation approaches have played an important role in interpreting the experimental results whilst capturing the major factors that control the overall mechanical responses of MoS_2.

School of Science, Harbin Institute of Technology, Shenzhen 518055, China. E-mail: jinzhang@hit.edu.cn

† Electronic supplementary information (ESI) available: Details about determination of the Young's modulus and hardness from indentation load–depth curves; parameters in the LJ potential; indentation load–depth curve of the pure SiO_2 substrate; evolution of Young's modulus and hardness of the MoS_2/SiO_2 system, graphene/SiO_2 system and pure SiO_2 substrate measured during the nanoindentation process; stacking patterns of multilayer MoS_2 and graphene; FE model of 2D material/substrate systems. See DOI: https://doi.org/10.1039/d2cp00074a

‡ These authors contributed equally.

As mentioned above, most existing studies have focused mainly on the mechanical properties of freestanding MoS_2. Nevertheless, 2D materials in practical applications are usually mounted on a substrate [*e.g.*, silicon dioxide (SiO_2), polyethylene terephthalate, and poly-dimethylsiloxane (PDMS)], which constitute the fundamental functional components of many nanodevices such as ultrathin electronic skins[27,28] and field-effect transistors.[29,30] So far, the mechanical behaviour of graphene mounted on various substrates has been widely investigated using nanoindentation experiments and simulations.[31–37] The results have shown that the interaction between graphene and the substrate can greatly affect the mechanical properties of graphene and its applications. Thus, it is reasonable to expect that the substrate may similarly have an impact on the mechanical behaviour and failure mechanisms of supported MoS_2. However, in spite of a very recent AFM-based nanoindentation study on the elastic behaviour of MoS_2 supported on flexible PDMS,[38] few studies have been carried out to investigate the mechanical responses of the supported MoS_2, especially for MoS_2 mounted on a stiff substrate such as SiO_2.

In this work, the deformation behaviour together with the mechanical properties of multilayer MoS_2 mounted on the SiO_2 substrate are investigated using nanoindentation experiments and MD simulations. For the sake of comparison, the graphene/SiO_2 system is also studied using similar experiments and simulations. Here, the nanoindentation experiments are conducted to reveal the relationship between the 2D material/substrate interactions and the overall mechanical responses of the MoS_2/SiO_2 or graphene/SiO_2 system, since nanoindentation has the ability to correlate the molecular-level properties of materials with their micro/macroscopic events, which has been previously applied to many other thin-film materials such as organic crystals.[39–41] On the other hand, it is difficult to use experiments themselves for automatically revealing the physics behind the observed behaviour. Thus, MD simulations are necessary for understanding the deformation mechanisms of material interfaces.[42] In general, the MoS_2/SiO_2 and graphene/SiO_2 systems are found to possess similar mechanical properties but exhibit very different types of deformation behaviour. Specifically, a unique interface delamination failure is observed in the MoS_2/SiO_2 system with a relatively thin MoS_2 layer. The delamination mechanism of the MoS_2/SiO_2 system is revealed using MD simulations and the continuum mechanical analysis. This work is anticipated to provide beneficial guidance for the rational design of nanodevices that incorporate components of the MoS_2/SiO_2 system.

Results and discussion

Fig. 1(a) shows a schematic overview of the sample preparation, which was implemented through mechanical exfoliation. As shown in Fig. 1(b), the thickness of the mechanically exfoliated MoS_2 flake mounted on the SiO_2 substrate varies in different regions of the flake. The thickness of the different regions of the MoS_2 flake can be determined *via* the AFM micrograph, as shown in Fig. 1(c), in which a clear interface between MoS_2 and

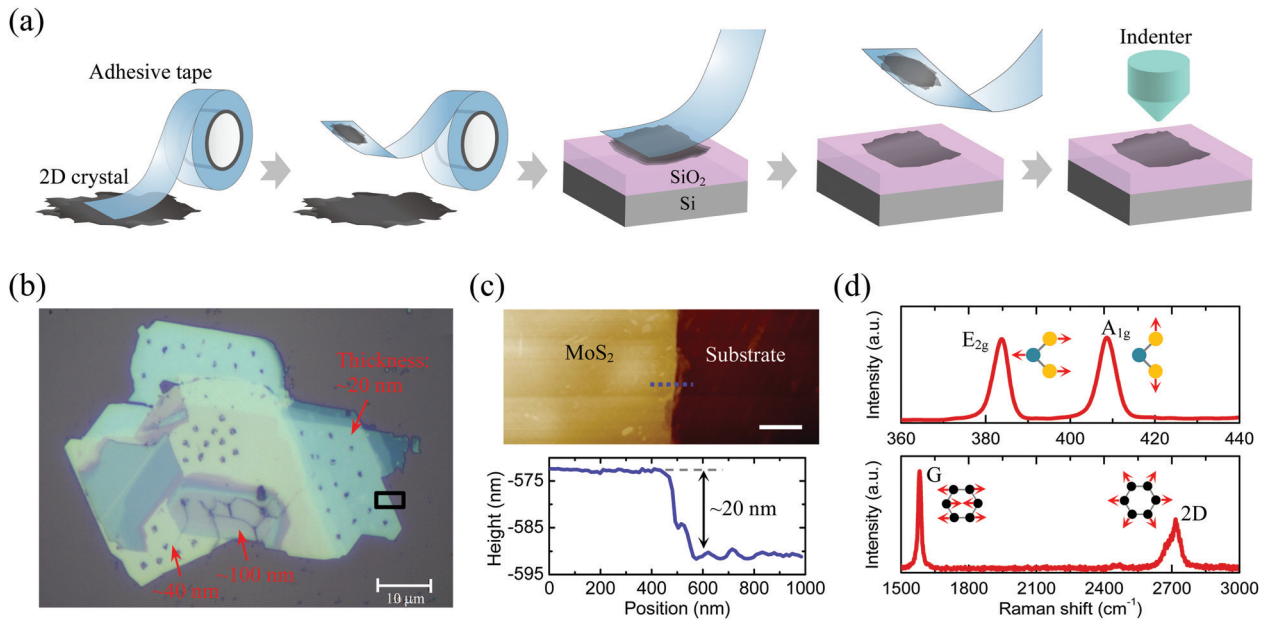

Fig. 1 Sample preparation. (a) Micromechanical exfoliation of multilayer 2D materials (MoS_2 and graphene) for nanoindentation experiments. (b) A typical optical microscopy image of a supported MoS_2 flake after the nanoindentation experiments. Here, indentations are carried out in different regions of the MoS_2 flake to investigate the effect of the MoS_2 thickness. (c) (top) AFM image of the region outlined by the rectangular box in (b), and (bottom) the corresponding height profile topography image along the dashed blue line of the AFM image. The scale bar is 1 μm. (d) Raman spectra of 20-nm-thick MoS_2 (top) and graphene (bottom) mounted on the SiO_2 substrate. The red arrows in the insets indicate the direction of the movement of Mo, S and C atoms.

the SiO_2 substrate is observed. Through indenting different regions of the MoS_2 flake, we can investigate the effect of the flake thickness on the mechanical properties of supported MoS_2. For the sake of comparison, our study also considers multilayer graphene mounted on the SiO_2 substrate, the experimental samples of which were prepared using a similar mechanical-exfoliation method. Raman spectra were employed for the qualitative spectroscopic characterization of the transferred MoS_2 and graphene. As shown in Fig. 1(d), the peaks of MoS_2 are located at 383.9 cm^{-1} and 405.4 cm^{-1}, which correspond to the in-plane E^1_{2g} and out-of-plane A_{1g} phonon modes of MoS_2, respectively. The uniform Raman signal intensity shown in Fig. 1(d) confirms the high purity and quality of the transferred MoS_2 thin films. Moreover, the excellent crystallinity is similarly confirmed for the transferred graphene thin films on the SiO_2 substrate, since, as shown Fig. 1(d), their Raman spectrum exhibits high-intensity G and 2D peaks, respectively, at ~1580 cm^{-1} and ~2700 cm^{-1}.

Fig. 2 shows the typical indentation load–depth curves of supported MoS_2 and graphene thin films of the same thickness. Here, samples with different thicknesses of ~20, ~40, and ~100 nm were considered for both MoS_2 and graphene samples. All load–depth curves have an initial elastic segment due to the initial elastic contact in the indentation process, which can be theoretically described using Hertzian contact theory.[43] Afterwards, a pop-in event leading to a plateau associated with a sudden finite penetration is observed in the load–depth curves. Similar nanoindentation tests were also performed for the pure SiO_2 substrate. The obtained indentation load–depth curve of pure SiO_2 is shown in Fig. S1 (ESI†), in which no detectable pop-in events are observed. This result indicates that the pop-in events occurring in the 2D material/SiO_2 systems may originate predominantly from the failure of the 2D material itself and/or the failure of the interface between the 2D material and the substrate. The pop-in events are found to be strongly dependent on the thickness of the 2D material. As for MoS_2 with a thickness of ~20 nm, only one pop-in event is observed at a load of 0.12 mN. When the thickness of MoS_2 is increased to ~40 nm, although the first pop-in event is similarly observed at a load of around 0.10 mN, two further pop-in events are sequentially observed as the indentation load is increased. Specifically, the length of the third pop-in is very much larger than that of the previous two, which indicates that the final pop-in event should have a different mechanism. More pop-in events are observed in the MoS_2/SiO_2 system when the thickness of the component MoS_2 layer is increased to ~100 nm. Specifically, the first pop-in is now found at a load of 0.3 mN, which is totally different from the value of ~0.10 mN observed for the MoS_2 thickness of ~20 or ~40 nm. This result indicates that the deformation mechanism of thick MoS_2 (with a thickness of ~100 nm) mounted on SiO_2 could be different from that of its thin counterparts (with a thickness of ~20 or ~40 nm). When compared with MoS_2, a much simpler pop-in phenomenon is observed in the graphene/SiO_2 system. For example, there is only one obvious pop-in event observed in all graphene/SiO_2 systems considered here, although the pop-in length and the indentation load at the pop-in of supported graphene with a thickness of ~100 nm are both larger than those of its counterparts with thicknesses of ~20 and ~40 nm. From the above results, we can come to the conclusion that, compared with its graphene counterpart, a more complex deformation mechanism occurs in supported MoS_2 upon indentation, which can become more significant as the MoS_2 thickness is increased. The pop-in mechanism or deformation mechanism of supported MoS_2 with different thicknesses will be discussed later.

The morphologies of the MoS_2/SiO_2 and graphene/SiO_2 systems after indentation were investigated *via* scanning

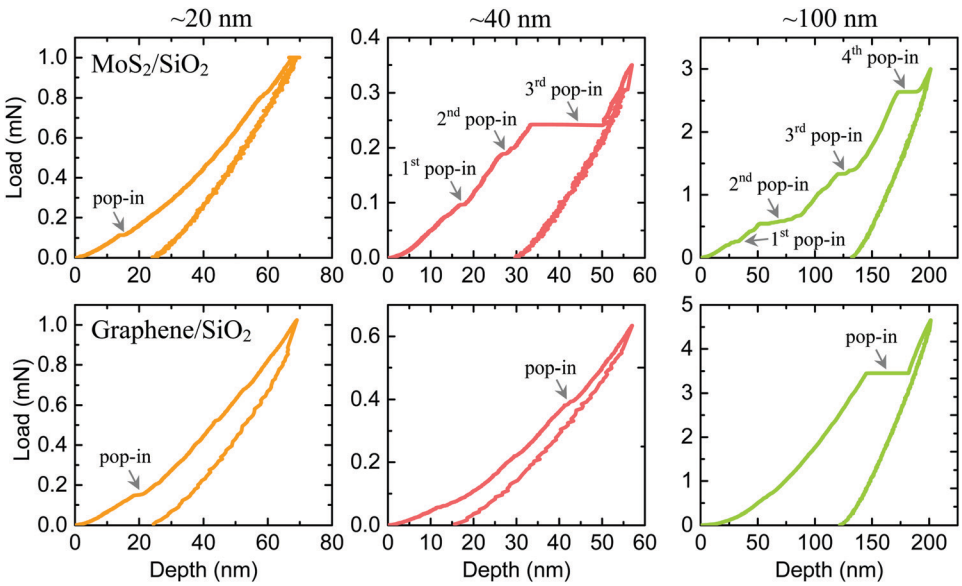

Fig. 2 Indentation load–depth curves for the MoS_2/SiO_2 system (top panels) and graphene/SiO_2 system (bottom panels) with different MoS_2 and graphene thicknesses (~20, ~40, and ~100 nm).

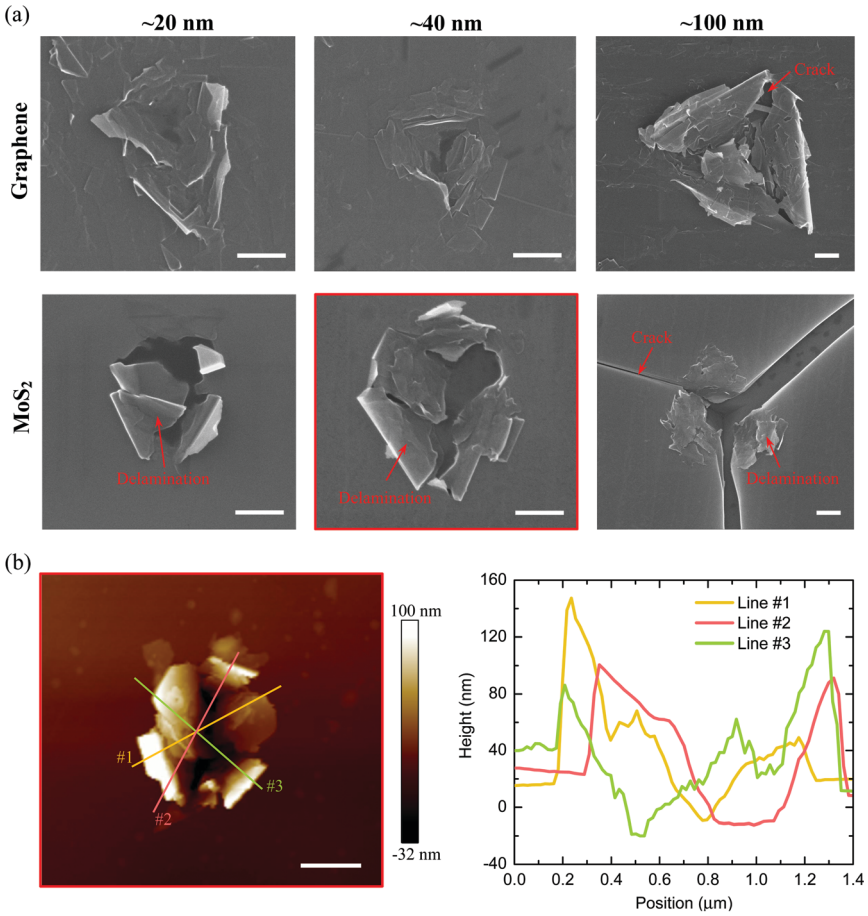

Fig. 3 Morphologies of the 2D material/SiO_2 systems after the nanoindentation experiments. (a) SEM images of the graphene/SiO_2 system (top panels) and MoS_2/SiO_2 system (bottom panels) with different MoS_2 and graphene thicknesses. Scale bars are 300 nm. (b) AFM image of the MoS_2/SiO_2 system whose MoS_2 component has a thickness of ~40 nm. The corresponding height profiles along the three lines are shown in the right topography image. The scale bar is 500 nm.

electron microscopy (SEM) as shown in Fig. 3(a). For the graphene/SiO_2 system with a graphene thickness of ~20 or ~40 nm, each layer of the supported graphene is penetrated due to the stress concentration generated by the indenter, which results in the layer-by-layer fracture of the supported graphene. A similar failure mode has been observed in recent experiments on freestanding two-layer graphene and supported 2D metal–organic frameworks indented using AFM.[44,45] Since most fractured graphene layers are not separated from the bulk graphene, no significant pop-in events will be observed in the corresponding indentation load–depth curves (see Fig. 2(a)). When the graphene thickness increases to ~100 nm, a visible radial through-thickness crack is observed at the contact edge between the indenter and graphene, which is responsible for the significant pop-in event observed in the indentation load–depth curve. It is noted that this failure mode is identical to that observed in most bulk materials under indentation.[46] Different from the layer-by-layer fracture of individual graphene layers in the graphene/SiO_2 system with a graphene thickness of ~20 or ~40 nm, an integrated fracture mode is observed in the supported MoS_2 component of the MoS_2/SiO_2 system for the MoS_2 thicknesses of ~20 and ~40 nm. Specifically, as shown in Fig. 3(a), in the MoS_2/SiO_2 system an interfacial crack is found in the region under the indenter, which is induced by delamination of the supported MoS_2 thin film from the SiO_2 substrate. Moreover, through the AFM analysis shown in Fig. 3(b), in addition to the interfacial crack, a ring-like through-thickness crack is also observed in the MoS_2 thin film, since a sudden and significant thickness drop is observed at the end of the delaminated MoS_2 thin film. This ring-like through-thickness cracking could be responsible for the significant pop-in events observed in the indentation load–depth curves of the corresponding MoS_2/SiO_2 systems. However, as the thickness of the MoS_2 component in the MoS_2/SiO_2 system is increased to ~100 nm, the failure of the MoS_2/SiO_2 system is found to be induced predominantly by radial through-thickness cracking, which is similar to the failure mode observed in the graphene/SiO_2 counterpart with the same graphene thickness. Meanwhile, for the MoS_2/SiO_2 system with the MoS_2 thickness of ~100 nm, the indentation process is accompanied by delamination between the layers of MoS_2 prior to the final cracking failure, which could be the factor inducing the

complex pop-in events in the corresponding indentation load–depth curves.

The evolution of the equivalent Young's modulus and hardness of the composite MoS_2/SiO_2 and graphene/SiO_2 systems measured during the indentation process is shown in Fig. S2 and S3 (ESI†), which were evaluated from the indentation load–depth curves *via* the Oliver–Pharr method (as described in the ESI†).[47] Thus, the equivalent Young's modulus and hardness calculated here contain contributions from both the supported 2D materials and the SiO_2 substrate. From Fig. S2 (ESI†) we can see that although the Young's modulus of graphene is much larger than that of its MoS_2 counterpart,[11] the equivalent Young's moduli of MoS_2/SiO_2 and graphene/SiO_2 systems are almost identical to each other, which are close to the value of around 90 GPa of the SiO_2 substrate (see Fig. S4, ESI†). Based on the theoretical model proposed previously,[33] this finding can be attributed to the fact that the supported MoS_2 or graphene layer has a much smaller thickness and also a larger Young's modulus compared with its SiO_2 substrate counterpart. Similarly, as shown in Fig. S3 (ESI†), the equivalent hardness of the overall MoS_2/SiO_2 and graphene/SiO_2 systems prior to failure is also found to be close to the value of around 10.5 GPa of the SiO_2 substrate (see Fig. S4, ESI†). These results indicate that the Young's modulus and hardness of the MoS_2/SiO_2 and graphene/SiO_2 systems considered here are dominated by their substrate, *i.e.*, SiO_2. Similar findings were also reported in previous nanoindentation experiments for graphene mounted on copper.[35] Moreover, the fracture of the supported MoS_2 and graphene layers is found to have different effects on the equivalent Young's modulus and hardness of the 2D material/SiO_2 systems. Specifically, the equivalent Young's modulus of both 2D material/SiO_2 systems after the fracture (or the occurrence of pop-in) can recover almost to the value before the fracture, which is irrespective of the thickness of the supported 2D material. However, a significant drop of the equivalent hardness can be observed in the 2D material/SiO_2 systems after the fracture, which is especially significant in the MoS_2/SiO_2 system where the MoS_2 layer has a thickness of $\sim$40 or $\sim$100 nm and the graphene/SiO_2 system where the graphene layer has a thickness of $\sim$100 nm. The drop of the equivalent hardness occurring in these 2D material/SiO_2 systems is induced by the radial through-thickness and/or ring-like through-thickness cracking of their supported MoS_2 and graphene layers, since the occurrence of these cracks can reduce the contact area and thus result in the underestimation of the equivalent hardness. In other words, the drop in the equivalent hardness observed during the indentation process for MoS_2/SiO_2 and graphene/SiO_2 systems can further prove that the significant pop-in events observed in their indentation load–depth curves are triggered by the radial through-thickness or ring-like through-thickness cracking of their supported MoS_2 and graphene layers.

To understand the different mechanical responses and failure modes observed between the MoS_2/SiO_2 and graphene/SiO_2 systems, especially when the MoS_2 and graphene components have a relatively small thickness, MD simulations were carried out for the nanoindentation of MoS_2 or graphene mounted on amorphous SiO_2. Ten-layer graphene and five-layer MoS_2 with almost the same thickness of $\sim$3.1 nm were considered in the present simulations. Fig. 4(a) shows the calculated force–displacement curves of the MoS_2/SiO_2 and graphene/SiO_2 systems. It is found that when the displacement of the indenter increases to $\sim$9 Å, the force starts to grow from zero, which indicates the onset of contact between the diamond indenter and MoS_2 (or graphene) through vdW interactions. Afterwards, both 2D material/SiO_2 systems experience a similar short elastic deformation period in which the relationship between the force and displacement follows Hertz's model.[43] However, as the displacement of the indenter continues to increase, some sharp force drops are observed in the force–displacement curves, which correspond to the failure of the supported 2D materials. Fig. 4(a) also shows that, compared with the graphene/SiO_2 system, the MoS_2/SiO_2 system requires a much lower force to achieve the same penetration depth, which indicates the smaller hardness of the MoS_2/SiO_2 system. This simulation result is consistent with the above experimental finding. In Fig. 4(b), we show the morphologies of supported MoS_2 and graphene after complete unloading. As the indenter can penetrate through the entire graphene and MoS_2 thin films during the indentation process, both the graphene and MoS_2 thin films are similarly broken at the edges of the indentation. Moreover, significant out-of-plane displacements are observed in the MoS_2 thin film, which, however, are absent from its graphene counterpart. This morphological difference indicates that the supported graphene thin film under indentation can adhere well to the SiO_2 substrate, while its MoS_2 counterpart under the same indentation conditions can be detached from the substrate. The morphologies of supported MoS_2 and graphene extracted from MD simulations are identical to those observed in the experiments, which further proves the delamination of supported MoS_2 thin films observed in the experiments.

In Movies 1 and 2 (ESI†), we show the evolution of morphologies of MoS_2/SiO_2 and graphene/SiO_2 systems, respectively, during the whole process of MD-based nanoindentation simulations. Meanwhile, some representative snapshots at different indenter displacements are shown in Fig. 4(c). Prior to the indentation, MoS_2 and graphene thin films adhere flatly to the SiO_2 substrate due to the effect of vdW interactions. When the indenter initially contacts the MoS_2 and graphene thin films, *e.g.*, at the displacement of 20 Å, the films deform elastically. When the indenter moves to a larger displacement of 40 Å, some upper layers in both the MoS_2 and graphene thin films are broken by the indenter. As the displacement of the indenter is increased further, the remaining layers in the 2D material thin films are broken sequentially until complete penetration of the indenter. This layer-by-layer breaking of the thin films is responsible for the many sharp force drops observed in the corresponding force–displacement curves. During the penetration process, the graphene thin film is found always to adhere to the SiO_2 substrate, while delamination from the substrate is observed in the supported MoS_2 thin film, which can be

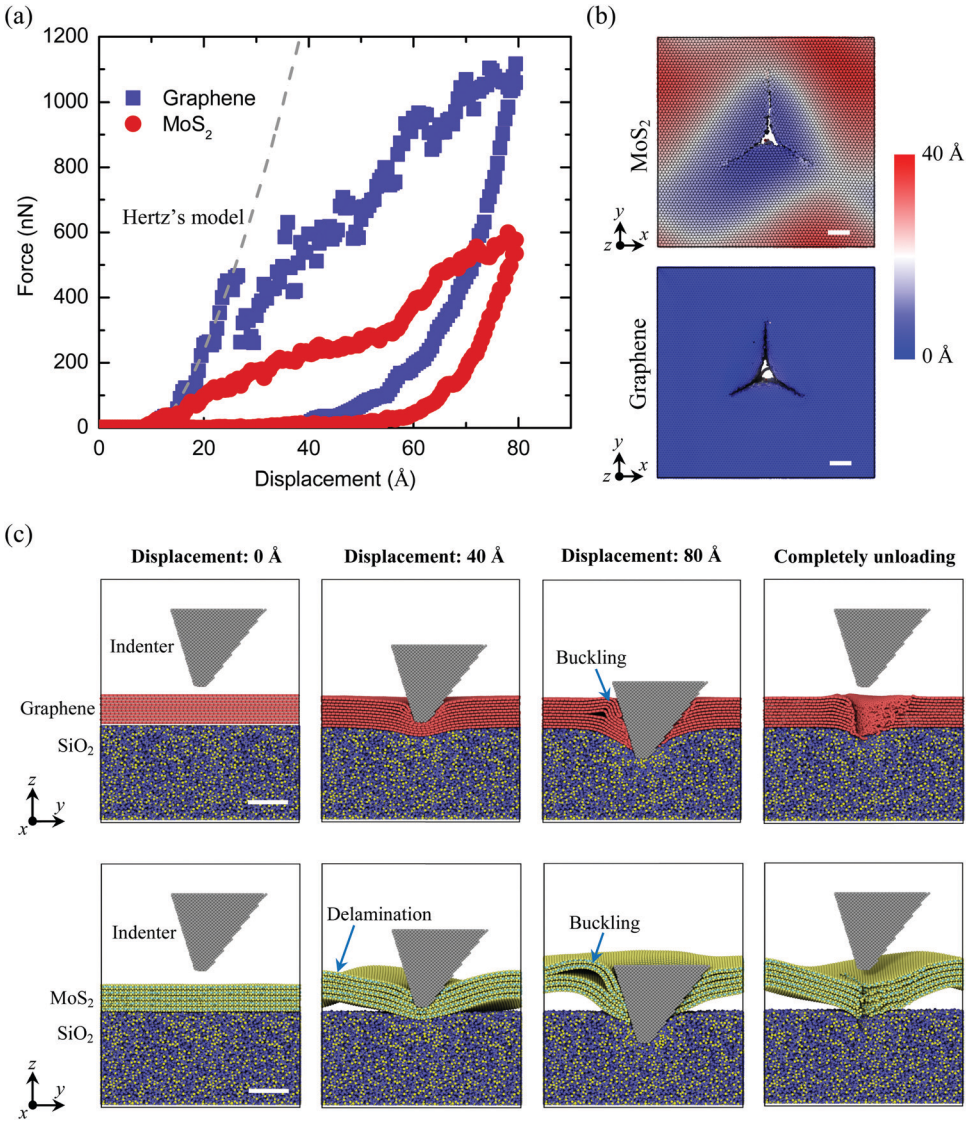

Fig. 4 MD-based nanoindentation simulations for the 2D material/SiO_2 systems. (a) Force–displacement curves of 10-layer graphene and 5-layer MoS_2 mounted on the SiO_2 substrate. The results follow Hertz's model at the early indentation stage. (b) Out-of-plane deformation patterns of the covered MoS_2 and graphene layers after the indentation. Here, atoms of each layer are coloured according to their vertical height with respect to the centre of mass of the layer. Scale bars are 2 nm. (c) Representative MD simulation snapshots of the graphene/SiO_2 system (top panels) and MoS_2/SiO_2 system (bottom panels) during the whole nanoindentation simulation process. Scale bars are 4 nm.

retained even after complete release of the indentation load. This result indicates that delamination of the MoS_2/SiO_2 interface is induced in the loading process rather than the unloading process of indentation. Due to the delamination of the MoS_2 thin film from the SiO_2 substrate, the load-bearing area of the MoS_2/SiO_2 system under indentation is much smaller than that of its graphene/SiO_2 counterpart, which could be another factor causing the lower hardness of the MoS_2/SiO_2 system after the fracture of the supported MoS_2 layer. In addition, during the loading process of indention, some component layers in graphene and MoS_2 are pushed by the edges of the indenter, which leads to the buckling of these component layers. Moreover, the buckling phenomenon in MoS_2 is more significant than that in graphene. This significant buckling effect in MoS_2 may induce delamination between the layers of MoS_2 under indentation, as observed in the nanoindentation experiments of the MoS_2/SiO_2 system where the MoS_2 thickness is $\sim$100 nm.

In order to better demonstrate the delamination mechanism of the MoS_2/SiO_2 system, we carried out continuum mechanical analysis. As shown in MD simulations, the delamination of the MoS_2/SiO_2 interface originates basically from the out-of-plane deformation of MoS_2 during the loading process of indentation, which is induced by the bending of MoS_2. To verify whether or not a bending force is generated in the supported MoS_2 thin film under indentation, in Fig. 5(a) we show the distribution of its bending moment, as simulated using finite element (FE) calculations. For the sake of comparison, the result of the supported graphene thin film with the same

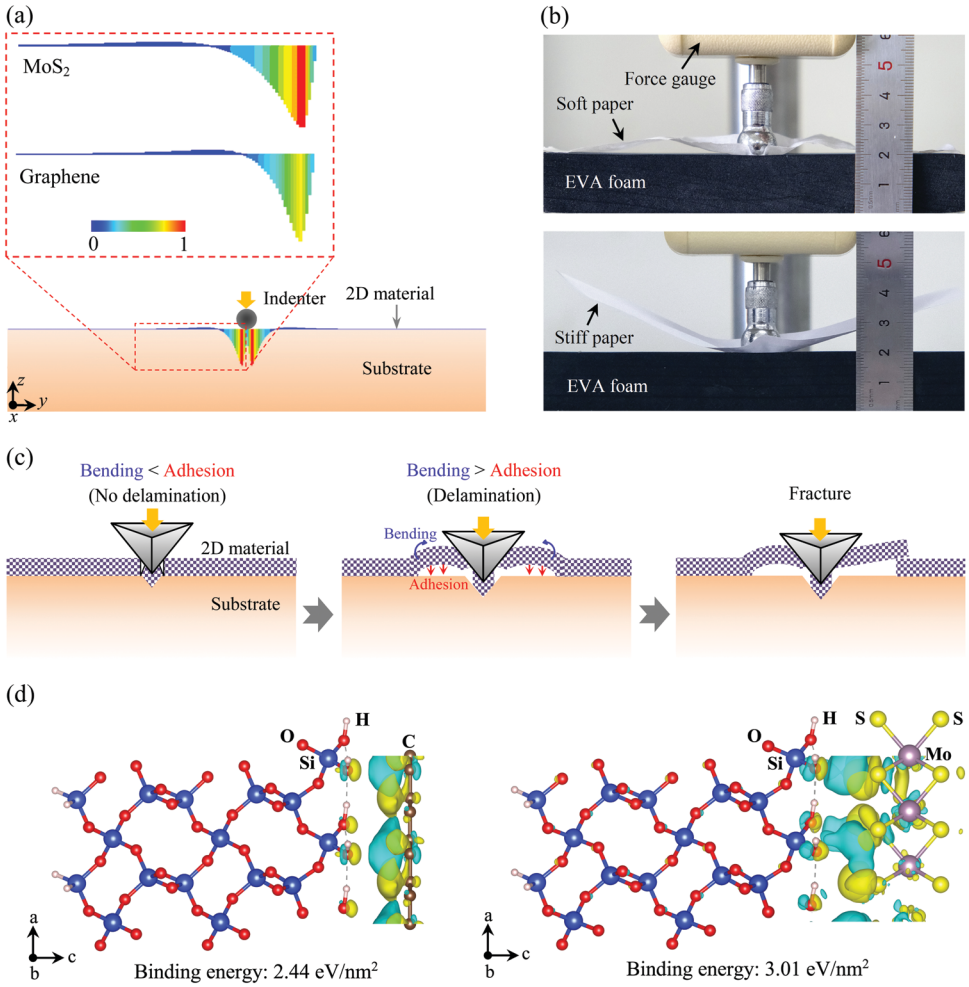

Fig. 5 Deformation mechanism of the supported 2D materials under indentation. (a) Bending moment distribution in supported MoS_2 and graphene thin films obtained from FE calculations. Here, results are normalized by the maximum value of MoS_2. (b) The out-of-plane deformation of a soft paper sample (analogous to graphene) and a stiff paper sample (analogous to MoS_2) laid on the surface of EVA foam. Here, both samples are indented to the same depth. (c) Schematic of various representative stages in the nanoindentation of a 2D material/SiO_2 system. The competition between the bending effect generated in the 2D material under indentation and the adhesion (vdW) effect of the 2D material/SiO_2 interface results in the different deformation mechanisms and failure modes observed in the MoS_2/SiO_2 and graphene/SiO_2 systems under indentation. (d) Local electron density difference and binding energy of the graphene/SiO_2 interface (left) and MoS_2/SiO_2 interface (right).

thickness and under the same indentation depth is also shown here. Indeed, the bending moment is found to exist in a small area of the thin film around the indenter. Moreover, the acting area and the magnitude of the bending moment in MoS_2 are both larger than those in the graphene counterpart, which can be attributed to the much larger bending stiffness of MoS_2. For the MoS_2 and graphene thin films (with the same thickness of 20 nm) considered in the FE calculations, the bending stiffness of MoS_2 ($\sim 9 \times 10^{-14}$ Nm) is more than four times larger than that of its graphene counterpart ($\sim 2 \times 10^{-14}$ Nm).[17] The result extracted from FE calculations is further validated using an analogical macroindentation experiment for paper samples of different stiffnesses depicted in Fig. 5(b), in which papers are bent upwards by the indenter. Furthermore, the tilting is found to be more significant in the paper with the higher bending stiffness, which indicates that a larger bending effect can be generated in a thin film with a higher bending stiffness. From the above analysis, we can deduce that the bending moment can be generated in the supported 2D materials during the indentation process, and that the more significant bending effect in the MoS_2 thin film could be the factor that induces delamination of the MoS_2 thin film from the SiO_2 substrate.

In Fig. 5(c), we schematically show representative stages in the nanoindentation process for the 2D material/SiO_2 systems. At an early stage with a small indentation load, the 2D material can be broken by the very high stresses in the contact area, especially the tensile stresses at the contact edges, because the indenter is rather sharp and the contact area is very small. Although the indentation can simultaneously generate the bending moment in the 2D material, at this early stage, the bending in the 2D material is too small to overcome the interfacial adhesion (vdW interactions) between the 2D material and the substrate. Thus, no delamination will occur. With a growing indentation depth, the bending effect in the 2D

material will increase. If the bending energy in this process is always smaller than the adhesion energy, the 2D material can adhere well to the substrate during the whole indention process. However, if the bending energy in the 2D material at a certain indentation depth becomes larger than the adhesion energy of the 2D material/SiO_2 interface, the 2D material near the indenter will bulge upwards leading to its delamination from the SiO_2 substrate. Furthermore, as the indentation depth keeps increasing, the height of the bulged 2D material increases. When the height reaches a critical value, the bending stress in the bulged 2D material around the indenter will result in the formation of a ring-like through-thickness crack as observed in the MoS_2/SiO_2 system for the MoS_2 thicknesses of ~20 and ~40 nm (see Fig. 3(a) and (b)). These fragmented parts will be stacked on the remaining 2D material thin film due to the vdW interactions between them. Based on this proposed mechanism, the different failure modes observed between the MoS_2/SiO_2 and graphene/SiO_2 systems can be explained, and are attributed to the different abilities of their 2D material layers to overcome their interfacial adhesion. To evaluate the binding energy for the MoS_2/SiO_2 and graphene/SiO_2 interfaces, density functional theory (DFT) calculations were performed. Here, the binding energy ΔE was calculated through $\Delta E = (E_{T\text{–}S} - E_T - E_S)/A$, where E_T, E_S, and $E_{T\text{–}S}$ are the energy values of the isolated 2D material (MoS_2 or graphene), the SiO_2 substrate, and the 2D material/SiO_2 system, respectively, and A is the contact area between the 2D material and the SiO_2 substrate. The binding energies of the MoS_2/SiO_2 and graphene/SiO_2 interfaces are 3.01 and 2.44 eV nm^{-2}, respectively. The slightly larger binding energy of the MoS_2/SiO_2 system can be attributed to the larger charge accumulation and stronger electron interaction in the MoS_2/SiO_2 interface, as shown in Fig. 5(d). Actually, the similar comparable binding energy (adhesion energy) of the MoS_2/SiO_2 and graphene/SiO_2 systems was also observed in previous experiments.[48] Although the MoS_2/SiO_2 and graphene/SiO_2 interfaces have a comparable adhesion energy, the bending stiffness of MoS_2, as mentioned above, is much larger than that of its graphene counterpart, which means that MoS_2 experiences a larger bending energy during the indentation process. Thus, the indented MoS_2 has a greater capacity to resist the adhesion of the MoS_2/SiO_2 interface, resulting in the easier delamination of the MoS_2 thin film from the SiO_2 substrate.

Conclusions

In conclusion, the mechanical properties and deformation behaviour of multilayer MoS_2 mounted on the SiO_2 substrate were investigated using nanoindentation experiments and MD simulations. For the sake of comparison, similar experiments and simulations were also performed for the graphene/SiO_2 system. The Young's modulus and hardness of the MoS_2/SiO_2 system were found to be comparable to those of its graphene/SiO_2 counterpart, though the mechanical properties of MoS_2 are much weaker than those of graphene. However, totally different mechanical responses and failure modes were observed in the MoS_2/SiO_2 and graphene/SiO_2 systems under indentation, especially when the MoS_2 and graphene thin films are relatively thin. Specifically, a unique delamination failure accompanied by the ring-like through-thickness cracking was observed in the supported MoS_2 layer of the MoS_2/SiO_2 system during the loading process of indentation, while no interface separation was found in the graphene/SiO_2 system under indentation. It was revealed that delamination of the MoS_2 thin film from the SiO_2 substrate can be attributed to the very large bending stiffness of MoS_2, which can induce a large bending effect in MoS_2 during the indentation process and thus give it a great capacity to overcome the adhesion of the MoS_2/SiO_2 interface. Overall, our study comprehensively reveals the mechanical response and failure mode of 2D materials (MoS_2 and graphene) mounted on a stiff substrate (SiO_2), which are of fundamental importance for the rational design of nanodevices so as to avoid the fracture failure of their 2D material/SiO_2 components.

Methods

Sample preparation

Multilayer MoS_2 thin films were mechanically exfoliated from commercially available MoS_2 crystals (SixCarbon Technology Shenzhen) and positioned onto the SiO_2/Si substrate using Scotch tape as the transfer medium. Before exfoliating, the substrates were cleaned sequentially in acetone, ethanol and de-ionized water. Afterwards, oxygen plasma treatment was performed to further remove ambient adsorbates on the substrate surface. Mechanical exfoliation was implemented using the following procedure. First, the tape was pressed to make contact with the MoS_2 crystals, which resulted in the adhesion of some MoS_2 flakes on the tape. Second, the first step was repeated several times to thin the flakes. Third, the substrate was pressed onto the tape and, sequentially, heated to a temperature of around 100 °C. Finally, after the sample temperature has cooled to ambient temperature, the tape was removed from the substrate slowly, which resulted in some thin MoS_2 flakes being left on the surface of the SiO_2 substrate. Graphene/SiO_2 samples were similarly obtained *via* the mechanical exfoliation of graphene from highly oriented pyrolytic graphite purchased from SixCarbon Technology Shenzhen.

Sample characterization

In order to characterise the 2D materials (MoS_2 and graphene) deposited on the SiO_2 substrate, Raman measurements were performed at room temperature using a Renishaw InVia Raman instrument with an Ar^+ laser (488 nm) with an incident power of ~0.25 mW and a spot size of ~1 μm. Meanwhile, the geometry of the transferred 2D materials was determined using an optical microscope (Leica DM2700 M) and AFM (Bruker Dimension Icon). Specifically, AFM scans in tapping mode were utilized for the topography analysis of the 2D materials on SiO_2

before and after nanoindentation. In addition, the surface morphology of the 2D material/SiO_2 systems after the nanoindentation experiments was also analysed using an SEM (Thermo Fisher Scientific Apreo 2) operated at 10.0 kV.

Nanoindentation

The nanoindentation tests for the 2D material/SiO_2 systems were conducted using the continuous stiffness measurement (CSM) mode of a nanoindentation system G200X (KLA) equipped with a diamond Berkovich indenter with a tip radius of ~20 nm. Before and after each indentation test, the indenter tip was calibrated using a standard silica sample. Meanwhile, the thermal drift was kept below ±0.05 nm s^{-1}. In the nanoindentation tests, the indenter was gradually loaded to a specific depth with a strain rate of 0.05 s^{-1} and then unloaded using the same rate. In order to generate statistically valid data, ten tests with the same indentation depth were performed at different positions on 2D materials with the same thickness. The spacing between each indentation was ten times the indentation depth, to avoid any influence of the indentation stress field.

Macroindentation

Macroindentation tests for paper samples with different bending stiffnesses were conducted using a force gauge (SHSIWI) equipped with a spherical indenter with a diameter of 1 cm. Before carrying out the indentation, two paper samples with the same geometry but different bending stiffnesses were placed on 2-cm-thick ethylene vinyl acetate (EVA) foam stuck to a flat base. The indenter was placed above the middle point of the papers and, afterwards, indented into the two paper/foam systems with the same displacement of 0.2 cm. The displacement of the indenter was monitored using a slide gauge.

MD simulations

All MD simulations were carried out utilizing the LAMMPS package.[49] In the simulations, 5-layer MoS_2 and 10-layer graphene were placed on the amorphous SiO_2 substrate with dimensions of 20 × 20 × 10 nm, while a cube corner diamond indenter with a height of 8 nm was placed above the top layer of the suspended 2D materials. Here, multilayer MoS_2 and graphene, respectively, have the AA′ and AB stacking modes, as shown in Fig. S5 (ESI†). The interaction between the C atoms in the diamond indenter and the individual graphene layer was described *via* the adaptive intermolecular reactive empirical bond-order (AIREBO) potential,[50] while the Mo–S, Mo–Mo, and S–S interactions in an individual MoS_2 layer were described *via* the reactive empirical bond-order (REBO) potential.[51] The atomic interactions between the Si and O atoms in amorphous SiO_2 were described *via* the Tersoff potential.[52,53] The long-range vdW forces acting between adjacent layers of the 2D materials, between the indenter and the uppermost layer of the 2D material, and between the SiO_2 substrate and the lowermost layer of the 2D material were described *via* the Lennard-Jones (LJ) 12-6 potential together with the Lorentz–Berthelot mixing rules.[54] The LJ parameters for interactions between different systems are listed in Table S1 (ESI†). The whole simulation process contains the generation of an amorphous SiO_2 substrate and the subsequent nanoindentation. To generate the amorphous SiO_2 substrate, the temperature of the initially generated crystalline SiO_2 system was first increased using the Nosé–Hoover thermostat from 300 K to 5000 K (above the melting point) at 100 ps. At the temperature of 5000 K, the SiO_2 system was equilibrated for 50 ps. Afterwards, the system was quenched from 5000 K to 300 K in 1 ns. Finally, the system at 300 K and zero pressure was relaxed in the barostat (*NPT*) ensemble for 50 ps to obtain the equilibrium state of amorphous SiO_2. The nanoindentation simulations were implemented using the following procedure. First, the 2D material/SiO_2 system at room temperature (300 K) was relaxed within the canonical (*NVT*) ensemble for 50 ps to allow the system to reach the equilibrium state. Second, atoms in a thin layer with a thickness of 2 nm located at the bottom of SiO_2 substrate were fixed by setting their velocities and forces to zero to avoid boundary effects during the indentation process. The other atoms were set as Newtonian atoms, whose motion obeys Newton's second law and was integrated through a Velocity–Verlet algorithm. Last, atoms in the indenter were moved downwards to the required indentation depth with a constant speed of 0.5 Å ps^{-1}. In all simulations, periodic boundary conditions were applied in the lateral (x and y) directions. The time step was set as 0.5 fs for the melt-quench simulations and 1.0 fs for the nanoindentation simulations. Visualization of the nanoindentation process was realized using OVITO software.[55]

FE calculations

The commercial code ANSYS was used to perform the FE calculations. To reduce the computation cost, a central symmetry model (see Fig. S6, ESI†) was developed for both the 2D material/substrate sample and the indenter tip. The radius of the indenter tip was 10 nm, while the 2D materials and the substrate had the same radius of 200 nm. The multilayer 2D materials and the substrate were assumed to have a thickness of 20 nm and 100 nm, respectively. The 2D material was supposed to be bonded perfectly with the substrate. The material of the substrate was SiO_2, with a Young's modulus and a Poisson's ratio of 70 GPa and 0.17, respectively.[20] The bending stiffness of the MoS_2 thin film was set as 9×10^{-14} Nm, while the value of the graphene thin film was set as 2×10^{-14} Nm.[17] The indenter was modelled by the TARGE169/CONTA172 element pair to represent the contact between the indenter and the 2D material. The 2D materials were modelled as the SHELL208 element, while the substrate was modelled as the PLANE182 element.

DFT calculations

All first-principles calculations were based on DFT, which was implemented using the Vienna ab initio simulation package (VASP) code.[56] We adopted the generalized gradient approximation (GGA) for the electron exchange and the PBE+D3 functional,[57,58] which includes vdW forces. A supercell with the monolayer MoS_2 or monolayer graphene placed on α-quartz

was considered here. Using the Monkhorst–Pack sampling scheme,[59] a k-point mesh of $3 \times 3 \times 1$ was used for the sample. Due to the lattice mismatch between MoS_2 and SiO_2, 3×3 and 2×2 lateral supercells were selected for MoS_2 and SiO_2, respectively. Similarly, to reduce the lattice mismatch between graphene and SiO_2, 4×4 and 2×2 lateral supercells were selected for graphene and SiO_2, respectively. Six layers of SiO_2 were considered in the model, in which dangling bonds at the top and bottom surfaces of SiO_2 were fully passivated by hydrogen. Meanwhile, periodic boundary conditions were applied with a vacuum region of 15 Å along the out-of-plane direction to avoid interactions between adjacent supercells. The interface structures and atomic positions were fully optimized until the residual forces were less than 0.01 eV $Å^{-1}$.

Conflicts of interest

There are no conflicts to declare.

Acknowledgements

This work was supported by the National Natural Science Foundation of China (Grant No. 11602074) and the Natural Scientific Research Innovation Foundation in Harbin Institute of Technology (Grant No. HIT.NSRIF.2020058). Financial support from the Harbin Institute of Technology (Shenzhen Graduate School) through the Scientific Research Starting Project for New Faculty is gratefully acknowledged.

References

1 K. S. Novoselov, A. K. Geim, S. V. Morozov, D. Jiang, Y. Zhang, S. V. Dubonos, I. V. Grigorieva and A. A. Firsov, Electric field effect in atomically thin carbon films, *Science*, 2004, **306**, 666–669.
2 C. Tan, X. Cao, X.-J. Wu, Q. He, J. Yang, X. Zhang, J. Chen, W. Zhao, S. Han, G.-H. Nam, M. Sindoro and H. Zhang, Recent advances in ultrathin two-dimensional nanomaterials, *Chem. Rev.*, 2017, **117**, 6225–6331.
3 K. F. Mak, C. Lee, J. Hone, J. Shan and T. F. Heinz, Atomically thin MoS_2: A new direct-gap semiconductor, *Phys. Rev. Lett.*, 2010, **105**, 136805.
4 A. Splendiani, L. Sun, Y. Zhang, T. Li, J. Kim, C. Y. Chim, G. Galli and F. Wang, Emerging photoluminescence in monolayer MoS_2, *Nano Lett.*, 2010, **10**, 1271–1275.
5 M. Chhowalla, H. S. Shin, G. Eda, L.-J. Li, K. P. Loh and H. Zhang, The chemistry of two-dimensional layered transition metal dichalcogenide nanosheets, *Nat. Chem.*, 2013, **5**, 263–275.
6 B. Radisavljevic, A. Radenovic, J. Brivio, V. Giacometti and A. Kis, Single-layer MoS_2 transistors, *Nat. Nanotechnol.*, 2011, **6**, 147–150.
7 D. Jariwala, V. K. Sangwan, L. J. Lauhon, T. J. Marks and M. C. Hersam, Emerging device applications for semiconducting two-dimensional transition metal dichalcogenides, *ACS Nano*, 2014, **8**, 1102–1120.
8 R. Ganatra and Q. Zhang, Few-layer MoS_2: A promising layered semiconductor, *ACS Nano*, 2014, **8**, 4074–4099.
9 Q. He, Z. Zeng, Z. Yin, H. Li, S. Wu, X. Huang and H. Zhang, Fabrication of flexible MoS_2 thin-film transistor arrays for practical gas-sensing applications, *Small*, 2012, **8**, 2994–2999.
10 S. Hong, N. Zagni, S. Choo, N. Liu, S. Baek, A. Bala, H. Yoo, B. H. Kang, H. J. Kim, H. J. Yun, M. A. Alam and S. Kim, Highly sensitive active pixel image sensor array driven by large-area bilayer MoS_2 transistor circuitry, *Nat. Commun.*, 2021, **12**, 3559.
11 S. Bertolazzi, J. Brivio and A. Kis, Stretching and breaking of ultrathin MoS_2, *ACS Nano*, 2011, **5**, 9703–9709.
12 A. Castellanos-Gomez, M. Poot, G. A. Steele, H. S. van der Zant, N. Agrait and G. Rubio-Bollinger, Elastic properties of freely suspended MoS_2 nanosheets, *Adv. Mater.*, 2012, **24**, 772–775.
13 K. Liu, Q. Yan, M. Chen, W. Fan, Y. Sun, J. Suh, D. Fu, S. Lee, J. Zhou, S. Tongay, J. Ji, J. B. Neaton and J. Wu, Elastic properties of chemical-vapor-deposited monolayer MoS_2, WS_2, and their bilayer heterostructures, *Nano Lett.*, 2014, **14**, 5097–5103.
14 J. Jung, H. Bark, D. Byun, C. Lee and D.-H. Cho, Mechanical characterization of phase-changed single-layer MoS_2 sheets, *2D Mater.*, 2019, **6**, 025024.
15 Y. Manzanares-Negro, G. López-Polín, K. Fujisawa, T. Zhang, F. Zhang, E. Kahn, N. Perea-López, M. Terrones, J. Gómez-Herrero and C. Gómez-Navarro, Confined crack propagation in MoS_2 monolayers by creating atomic vacancies, *ACS Nano*, 2021, **15**, 1210–1216.
16 P. Huang, D. Guo, G. Xie and J. Li, Electromechanical failure of MoS_2 nanosheets, *Phys. Chem. Chem. Phys.*, 2018, **20**, 18374–18379.
17 G. Wang, Z. Dai, J. Xiao, S. Feng, C. Weng, L. Liu, Z. Xu, R. Huang and Z. Zhang, Bending of multilayer van der Waals materials, *Phys. Rev. Lett.*, 2019, **123**, 116101.
18 N. Iguiñiz, R. Frisenda, R. Bratschitsch and A. Castellanos-Gomez, Revisiting the buckling metrology method to determine the Young's modulus of 2D materials, *Adv. Mater.*, 2019, **31**, 1807150.
19 B. Graczykowski, M. Sledzinska, M. Placidi, D. Saleta Reig, M. Kasprzak, F. Alzina and C. M. Sotomayor Torres, Elastic properties of few nanometers thick polycrystalline MoS_2 membranes: A nondestructive study, *Nano Lett.*, 2017, **17**, 7647–7651.
20 Y. Li, C. Yu, Y. Gan, P. Jiang, J. Yu, Y. Ou, D.-F. Zou, C. Huang, J. Wang, T. Jia, Q. Luo, X.-F. Yu, H. Zhao, C.-F. Gao and J. Li, Mapping the elastic properties of two-dimensional MoS2 *via* bimodal atomic force microscopy and finite element simulation, *npj Comput. Mater.*, 2018, **4**, 49.
21 P. Li, C. Jiang, S. Xu, Y. Zhuang, L. Gao, A. Hu, H. Wang and Y. Lu, *In situ* nanomechanical characterization of multilayer MoS_2 membranes: From intraplanar to interplanar fracture, *Nanoscale*, 2017, **9**, 9119–9128.

22 J. Zhao, J.-W. Jiang and T. Rabczuk, Temperature-dependent mechanical properties of single-layer molybdenum disulphide: Molecular dynamics nanoindentation simulations, *Appl. Phys. Lett.*, 2013, **103**, 231913.
23 R. M. Elder, M. R. Neupane and T. L. Chantawansri, Stacking order dependent mechanical properties of graphene/MoS_2 bilayer and trilayer heterostructures, *Appl. Phys. Lett.*, 2015, **107**, 073101.
24 J.-W. Jiang, H. S. Park and T. Rabczuk, Molecular dynamics simulations of single-layer molybdenum disulphide (MoS_2): Stillinger-Weber parametrization, mechanical properties, and thermal conductivity, *J. Appl. Phys.*, 2013, **114**, 064307.
25 K. Q. Dang, J. P. Simpson and D. E. Spearot, Phase transformation in monolayer molybdenum disulphide (MoS_2) under tension predicted by molecular dynamics simulations, *Scr. Mater.*, 2014, **76**, 41–44.
26 S. Xiong and G. Cao, Bending response of single layer MoS_2, *Nanotechnology*, 2016, **27**, 105701.
27 M. Park, Y. J. Park, X. Chen, Y. K. Park, M. S. Kim and J. H. Ahn, MoS_2-based tactile sensor for electronic skin applications, *Adv. Mater.*, 2016, **28**, 2556–2562.
28 Y. J. Park, B. K. Sharma, S. M. Shinde, M. S. Kim, B. Jang, J. H. Kim and J. H. Ahn, All MoS_2-based large area, skin-attachable active-matrix tactile sensor, *ACS Nano*, 2019, **13**, 3023–3030.
29 Y. Guo, X. Wei, J. Shu, B. Liu, J. Yin, C. Guan, Y. Han, S. Gao and Q. Chen, Charge trapping at the MoS_2–SiO_2 interface and its effects on the characteristics of MoS_2 metal-oxide-semiconductor field effect transistors, *Appl. Phys. Lett.*, 2015, **106**, 103109.
30 Y. Park, H. W. Baac, J. Heo and G. Yoo, Thermally activated trap charges responsible for hysteresis in multilayer MoS_2 field effect transistors, *Appl. Phys. Lett.*, 2016, **108**, 083102.
31 J. Chen, X. Guo, Q. Tang, C. Zhuang, J. Liu, S. Wu and B. D. Beake, Nanomechanical properties of graphene on poly(ethylene terephthalate) substrate, *Carbon*, 2013, **55**, 144–150.
32 T. Niu, G. Cao and C. Xiong, Fracture behavior of graphene mounted on stretchable substrate, *Carbon*, 2016, **109**, 852–859.
33 Y. Zhang and C. Pan, Measurements of mechanical properties and number of layers of graphene from nanoindentation, *Diamond Relat. Mater.*, 2012, **24**, 1–5.
34 D. J. Kim, Q.-T. Truong, J. I. Kim, Y. Suh, J. Moon, S.-E. Lee, B. H. Hong and Y. S. Woo, Ultrahigh-strength multi-layer graphene-coated Ni film with interface-induced hardening, *Carbon*, 2021, **178**, 497–505.
35 S.-Y. Park, Y.-C. Kim, R. S. Ruoff and J.-Y. Kim, Incipient plasticity and fully plastic contact behavior of copper coated with a graphene layer, *APL Mater.*, 2019, **7**, 031106.
36 F. Bahrami, M. Hammad, M. Fivel, B. Huet, C. D'Haese, L. Ding, B. Nysten, H. Idrissi, J. P. Raskin and T. Pardoen, Single layer graphene controlled surface and bulk indentation plasticity in copper, *Int. J. Plast.*, 2021, **138**, 102936.
37 G. Cao and H. Gao, Mechanical properties characterization of two-dimensional materials *via* nanoindentation experiments, *Prog. Mater. Sci.*, 2019, **103**, 558–595.
38 H. Jiang, L. Zheng, Y. Wei and X. Wang, In-situ investigation of the elastic behavior of two-dimensional MoS_2 on flexible substrate by nanoindentation, *J. Phys. D: Appl. Phys.*, 2021, **54**, 504006.
39 K. Dey, S. Bhunia, H. S. Sasmal, C. M. Reddy and R. Banerjee, Self-assembly-driven nanomechanics in porous covalent organic framework thin films, *J. Am. Chem. Soc.*, 2021, **143**, 955–963.
40 S. Varughese, M. S. R. N. Kiran, U. Ramamurty and G. R. Desiraju, Nanoindentation in crystal engineering: Quantifying mechanical properties of molecular crystals, *Angew. Chem., Int. Ed.*, 2013, **52**, 2701–2712.
41 S. Mohata, K. Dey, S. Bhunia, N. Thomas, E. B. Gowd, T. G. Ajithkumar, C. M. Reddy and R. Banerjee, Dual nanomechanics in anisotropic porous covalent organic framework Janus-type thin films, *J. Am. Chem. Soc.*, 2022, **144**, 400–409.
42 W. J. Xia, J. Song, D. D. Hsu and S. Keten, Understanding the interfacial mechanical response of nanoscale polymer thin films *via* nanoindentation, *Macromolecules*, 2016, **49**, 3810–3817.
43 K. L. Johnson, *Contact Mechanics*, Cambridge University Press, Cambridge, UK, 1987.
44 Q.-Y. Lin, Y.-H. Zeng, D. Liu, G. Y. Jing, Z.-M. Liao and D. Yu, Step-by-step fracture of two-layer stacked graphene membranes, *ACS Nano*, 2014, **8**, 10246–10251.
45 Z. Zeng, I. S. Flyagina and J.-C. Tan, Nanomechanical behavior and interfacial deformation beyond the elastic limit in 2D metal–organic framework nanosheets, *Nanoscale Adv.*, 2020, **2**, 5181–5191.
46 A. C. Fischer-Cripps, *Nanoindentation*, Springer, New York, USA, 3rd edn, 2011.
47 W. C. Oliver and G. M. Pharr, An improved technique for determining hardness and elastic modulus using load and displacement sensing indentation experiments, *J. Mater. Res.*, 1992, **7**, 1564–1583.
48 Y. T. Megra and J. W. Suk, Adhesion properties of 2D materials, *J. Phys. D: Appl. Phys.*, 2019, **52**, 364002.
49 S. Plimpton, Fast parallel algorithms for short-range molecular dynamics, *J. Comput. Phys.*, 1995, **117**, 1–19.
50 S. J. Stuart, A. B. Tutein and J. A. Harrison, A reactive potential for hydrocarbons with intermolecular interactions, *J. Chem. Phys.*, 2000, **112**, 6472–6486.
51 T. Liang, S. R. Phillpot and S. B. Sinnott, Parametrization of a reactive many-body potential for Mo–S systems, *Phys. Rev. B: Condens. Matter Mater. Phys.*, 2009, **79**, 245110.
52 J. Tersoff, Modeling solid-state chemistry: Interatomic potentials for multicomponent systems, *Phys. Rev. B: Condens. Matter Mater. Phys.*, 1989, **39**, 5566–5568.
53 S. Munetoh, T. Motooka, K. Moriguchi and A. Shintani, Interatomic potential for Si–O systems using Tersoff parameterization, *Comput. Mater. Sci.*, 2007, **39**, 334–339.
54 D. Boda and D. Henderson, The effects of deviations from Lorentz-Berthelot rules on the properties of a simple mixture, *Mol. Phys.*, 2008, **106**, 2367–2370.
55 A. Stukowski, Visualization and analysis of atomistic simulation data with OVITO-the Open Visualization Tool, *Modell. Simul. Mater. Sci. Eng.*, 2010, **18**, 015012.

56 G. Kresse and J. Furthmüller, Efficient iterative schemes for ab initio total-energy calculations using a plane-wave basis set, *Phys. Rev. B: Condens. Matter Mater. Phys.*, 1996, **54**, 11169–11186.
57 J. P. Perdew, K. Burke and M. Ernzerhof, Generalized gradient approximation made simple, *Phys. Rev. Lett.*, 1996, **77**, 3865–3868.
58 S. Grimme, J. Antony, S. Ehrlich and H. Krieg, A consistent and accurate *ab initio* parametrization of density functional dispersion correction (DFT-D) for the 94 elements H-Pu, *J. Chem. Phys.*, 2010, **132**, 154104.
59 H. J. Monkhorst and J. D. Pack, Special points for Brillouin-zone integrations, *Phys. Rev. B: Condens. Matter Mater. Phys.*, 1976, **13**, 5188–5192.

